JOURNAL OF GEOPHYSICAL RESEARCH, VOL. 103, NO. D17, PAGES 22,073–22,085, SEPTEMBER 20, 1998

Chemical and microphysical properties of marine stratiform cloud in the North Atlantic

R.D. Borys, D.H. Lowenthal, and M.A. Wetzel

Atmospheric Sciences Center, Desert Research Institute, Reno, Nevada

F. Herrera and A. Gonzalez

Department of Fundamental and Experimental Physics, University of La Laguna, La Laguna, Canary Islands, Spain

J. Harris

NOAA Climate Monitoring and Diagnostics Laboratory, Boulder, Colorado

Abstract. The chemical and microphysical properties of marine stratiform cloud were measured at a ridgetop elevation of 992 m above mean sea level (AMSL) on Tenerife in the Canary Islands in the eastern North Atlantic during the summers of 1995 and 1996. The results show an inverse relationship between hourly-averaged cloud droplet diameter and droplet number concentration, which ranged from 116 to 1355 cm^{-3}. Strong relationships were observed between droplet number and equivalent clear air concentrations of non-sea-salt sulfate, nitrate, and elemental carbon in the droplets. Droplet sizes inferred from radiances measured by satellite for clouds offshore and upwind agreed with droplet sizes derived for clouds over the mountain sampling site, and also with those measured in cloud 4-5 hours later. Estimated cloud short-wave radiative forcing was enhanced by 8% in radiative model studies of polluted versus clean clouds with droplet concentrations of 786 and 127 cm^{-3} and droplet effective radii of 6 and 10 μm, respectively.

1. Introduction

Clouds play an important role in regulating global climate through heat and water transfer and by interacting with shortwave and longwave radiation. A crucial aspect of global climate change is the potential effect of anthropogenic aerosols on clouds. *Twomey* [1977] and *Twomey et al.* [1984] suggested that increases in anthropogenic or natural cloud condensation nuclei (CCN) would increase cloud droplet numbers, decrease droplet size, and increase cloud optical depth and albedo. This is the so-called "Twomey effect", and it may be similar in magnitude but opposite in sign to the "greenhouse effect", such that the reduction in the net flux of solar energy reaching the surface (a negative radiative forcing) due to increased globally averaged cloud albedo could counterbalance the atmospheric warming caused by greenhouse gases. Numerous estimates of changes in cloud radiative forcing due to the influence of anthropogenic aerosols have been made [e.g., *Charlson et al.*, 1992; *Jones et al.*, 1994; *Boucher and Lohmann*, 1995]. *Chuang et al.*[1997] estimated the average annual global cloud radiative forcing due to anthropogenic aerosol sulfate to be -0.6 to -1.6 W m^{-2}. The greatest uncertainty in the global radiation balance equation is our knowledge of the magnitude of the indirect effect of aerosols on clouds [*Schwartz and Andreae*, 1996].

Paper number 98JD02087.
0148-0227/98/98JD-02087 $09.00

Smaller droplet size may also inhibit the ability of clouds to precipitate by decreasing the efficiency of droplet growth by collision and coalescence [*Rogers and Yau*, 1989]. For a given cloud parcel, differences in cloud droplet size, or a broadening of the droplet size distribution, are required for precipitation initiation. *Albrecht* [1989] suggested a "secondary" Twomey effect, whereby an apparent enhancement of the liquid water content of polluted, nonprecipitating clouds relative to nonpolluted precipitating clouds would produce a larger increase in radiative forcing than would be expected just from increases in droplet numbers.

The number of droplets near cloud base has been shown to be directly related to the numbers of CCN entering the cloud. *Twomey and Warner* [1967] observed a correspondence between CCN at cloud base and cloud droplet number within 300 m of cloud base in nonprecipitating cumuli. Relatively high concentrations of aerosol particles produced augmented cloud droplet concentrations and smaller droplet sizes. The updraft velocity and CCN concentration determine the initial droplet distribution [*Warner*, 1969] which may later be altered by dynamical processes such as entrainment [*Baker et al.*, 1980] and evaporation and coalescence during convective mixing. Variations in the dynamics of cloud formation, as well as in the natural CCN population, contribute to variations in the droplet size distribution and other processes which may be droplet size dependent.

An experiment was conducted to relate long-term variations in marine stratus microphysical properties to variations in the concentrations of anthropogenic and natural chemical components

of the cloud water. Satellite observations were used to characterize the cloud structure at and upwind of the sampling area, to map aerosol optical depth in the vicinity of the clouds, and to make quantitative estimates of cloud droplet size. Case studies representing clean and polluted conditions were compared with respect to in situ and satellite-based measurements. Radiative transfer modeling was used to estimate broadband flux and albedo, and narrowband radiances were used to estimate cloud droplet size.

2. Experiment

Marine stratiform clouds (predominantly stratus, with some instances of stratocumulus) were sampled on the northeast, upwind side of the island of Tenerife in the Canary Islands in the eastern North Atlantic on 21 days from June 10 through July 7, 1995 and from July 4 through July 25, 1996. The sampling site, Pico del Ingles, is located on the summit of a ridge (28.50°N, 16.30°W) at an elevation of 992 m above mean sea level (AMSL). There were no significant island pollution sources upwind of the site. Clouds were sampled from a 10-m tower at night to avoid daytime ground-induced heating and resultant cloud dissipation and to minimize contamination from vehicular traffic. Cloud base was at most 200 m below the sampling site on any given sampling date, and the sampling location was at least 300 m below the top of the temperature inversion, well within the marine boundary layer (MBL) under typical trade wind conditions. The sampling site is located approximately 5.5 km southwest of the coast and local winds were always on-shore (from the northeast). The flow within the MBL was not impeded by the island at the study location. Air passed immediately from the upwind ocean region through the cloud over the local ridge, permitting access to clouds little affected by island aerosol sources.

Droplet size distributions were integrated continuously over 60-s intervals using a PMS FSSP-100 HV (forward scattering spectrometer probe) using range 1 (nominally 2 to 32 μm diameter). The FSSP was calibrated for each field season using the water-equivalent size of 2.1, 8.2, 15.7, 21.9, and 40 μm diameter glass microspheres (Duke Scientific Corporation). The calibrations corrected the FSSP size range to actual water droplet ranges of 2.4 to 23.8 μm diameter for the 1995 field season and 3.3 to 29.6 μm diameter for the 1996 field season. The regressions used to correct the raw data had $r^2 > 0.98$. Cloud liquid water content (LWC) was calculated from the FSSP size distributions. Errors in LWC estimate are related primarily to the uncertainties in the FSSP size determination and to a lesser extent the number concentration measurements. Based on the size calibration regression uncertainty, such errors are unrealistically small (<2%). The ground-based FSSP is not subject to sizing and sample area errors encountered at aircraft speeds. The same FSSP was used to measure cloud droplet size spectra and calculate cloud liquid water content in another mountaintop field program with the same 1995 calibration (R.D. Borys et al., The relationships among cloud microphysics, chemistry, and precipitation rate in cold mountain clouds, submitted to *Journal of Applied Meteorology*, 1998). A comparison of the FSSP-calculated LWC with an independent measure of LWC using cloud sieves [*Hindman et al.*, 1992] resulted in a correlation of 0.76, an average difference of -0.009 g/m^3 and a standard deviation of the difference of 0.06 g/m^3 for LWC values greater than 0.1 g/m^3. The difference between the two measures of LWC was not significant (paired t test). Thus the best estimate of the uncertainty in the calculated FSSP LWC is ±0.06 g/m^3. Cloud water was collected with a Caltech active strand cloud water collector (CASCC) [*Munger et al.*, 1989; *Collett et al.*, 1990]. The CASCC operated at a flow rate of 24.5 m^3/min with a strand diameter of 0.35 mm, producing a theoretical lower D_{50} cut point of 3.0 μm. Both instruments were mounted together and oriented into the wind with a large vane. A cloud water volume sufficient for detailed chemical analysis (>200 mL) was obtained in approximately 1 hour of sampling time. Mean diameter (MD, number-weighted mean) and droplet number concentrations were integrated over (approximately 1-hour) CASCC sample periods. Fifty-nine cloud water samples were obtained during the study. There were extended periods when no cloud was present, day or night. Wind speeds were monitored with a hand-held anemometer at a height of approximately 2.0 m.

Cloud water pH was measured directly within minutes after sampling. Samples were refrigerated in the field and frozen within 5 hours. Upon return to the United States, each sample was thawed and shaken, and 5 mL were withdrawn by syringe through a 1-cm^2 quartz fiber filter punch for analysis of insoluble elemental carbon (EC) by thermal-optical reflectance [*Chow et al.*, 1993]. Sulfate, nitrate, and chloride were analyzed by ion chromatography on a Dionex 4000i ion chromatograph with a Dionex AS4A column. Methanesulfonate (MSA) was analyzed separately on a Dionex 2020i ion chromatograph with an AS11 column. Soluble sodium was measured by flame atomic absorption on a Perkin Elmer Model 2380. Ammonium ion was measured by automated colorimetry using the indophenol method on a Technicon TRAACS 800 autoanalyzer.

Satellite multispectral data from the NOAA advanced very high resolution radiometer (AVHRR) instrument were collected by the University of La Laguna (ULL) and processed at ULL and the Desert Research Institute using SeaSpace TeraScan image analysis software. Calibrated image data from AVHRR provided pixel values at 1.1-km horizontal resolution for shortwave radiances in channel 1 (0.58-0.68 μm) and channel 2 (0.725-1.10 μm) and for equivalent blackbody temperatures in the near-infrared channel 3 (3.55-3.95 μm) and the two AVHRR thermal bands, channel 4 (10.3-11.3 μm) and channel 5 (11.5-12.5 μm). Cloud microphysical parameters were estimated by interpolating the satellite-derived cloud visible channel reflectance for AVHRR channel 1 and equivalent temperature in channel 3 to model-calculated values for a wide range of cloud droplet size, cloud depth, and Sun-target-satellite geometry [*Wetzel et al.*, 1996]. These model results were calculated using the streamer model [*Key*, 1996; *Meier et al.*, 1997] based on the discrete ordinates method [*Stamnes et al.*, 1988].

Isentropic back trajectories [*Harris and Kahl*, 1994] were used to identify potential sources of aerosols affecting the clouds sampled on Tenerife. Trajectories were calculated at 0000 and 1200 UT. Because sampling was usually begun at about 2000 UT, and continued for 4-5 hours, the 0000 UT trajectory on the following day corresponds most closely in time with the cloud sampling periods.

3. Results

3.1. Cloud Water Chemistry

The cloud water pH was consistently acidic, ranging from 3.0 to 4.4. Chemical concentrations in the droplets (ppm) were converted to clear air equivalent concentrations by multiplying by the LWC. All concentrations are subsequently reported as "clear air equivalent". This provides a surrogate measure of the precloud aerosol composition which is involved in the formation of the cloud. Ranges and means of concentrations of non-sea-salt sulfate (NSS), nitrate, ammonium, elemental carbon (EC), Na^+, Cl^-, and methanesulfonate (MSA) are given in Table 1. Second-year ammonium concentrations appeared significantly contaminated, by up to an order of magnitude compared with sulfate and nitrate, and are not included. NSS accounted for 75±15% of the total sulfate. The concentration of NSS sulfate ranged from 0.3 μg/m³, typical of the northern hemispheric marine background [*Bates et al.*, 1992], to 9.0 μg/m³, which is comparable to the average $PM_{2.5}$ (particles smaller than 2.5 μm in diameter) sulfate concentration measured in downtown Los Angeles [*Chow et al.*, 1994]. The average mass ratio of Cl/Na (1.83±0.20) reflected that of pure seawater (1.8) and the correlation between Na and Cl was 0.99. For the 1995 samples, the average ratio of measured ammonium to ammonium equivalent to NSS (as ammonium sulfate) plus ammonium equivalent to nitrate (as ammonium nitrate) was 0.38±0.10. The droplets therefore contained a significant amount of unneutralized sulfate and/or nitrate.

Nitrate and elemental carbon (EC) concentrations are plotted against those of NSS in Figures 1a and 1b, respectively. Nitrate and NSS concentrations were strongly correlated (r = 0.93). Excluding two outliers, EC and NSS concentrations were moderately correlated (r = 0.73). The higher variability in the EC-NSS relationship could be due in part to (1) the potential for inhomogeneity of the insoluble EC in suspension in the cloud water due to the sampling procedure (only 5 mL were withdrawn from the bulk sample); (2) differential absorption between samples of the hydrophobic EC particles on the walls of the sample bottle (although the sample bottle was shaken, surfactant was not added to the sample); and (3) differences in sources, transport, and incorporation in cloud droplets between primary (EC) and secondary (NSS) aerosol pollutants.

Table 1. Chemical Composition of Tenerife Cloud Water

Species	Mean±σ[a]	Range
NSS[b]	3.7±2.6	0.3-9.0
NO_3^-	2.1±1.2	0.2-5.0
NH_4^+[c]	1.00±0.60	0.2-2.4
EC	0.53±0.40	0.07-2.4
Na^+	3.5±2.6	0.5-14.2
Cl^-	6.5±5.5	1.01-29
MSA[d]	0.080±0.066	<0.02-0.47

Values are in micrograms per cubic meter.
[a] Average concentration and standard deviation.
[b] Non-sea-salt sulfate.
[c] Data from 1995 only.
[d] Methanesulfonate.

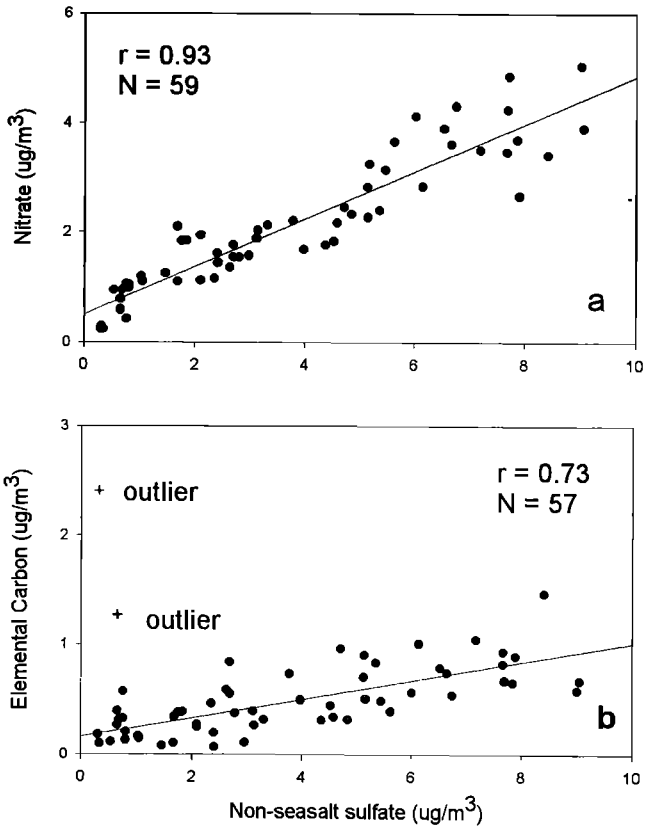

Figure 1. Cloud water clear air equivalent concentrations of non-sea-salt sulfate versus nitrate and elemental carbon.

3.2. Air Mass Back Trajectories

Six-day isentropic trajectories corresponding to each of the 21 sample days are plotted in sequence in Figure 2. The average daily NSS concentrations for each sample day are also shown. The high concentrations of NSS and nitrate in the cloud droplets suggest that the Canary Islands were strongly impacted by polluted air masses. In general, the trajectories and their associated NSS concentrations bear this out. High NSS concentrations on June 27, 1995 and July 19, 1996 are associated with trajectories which passed over western Europe. Conversely, the lowest NSS concentrations of the study were associated with trajectories from the west, that is, from the North Atlantic. There were no trajectories from Africa on cloud-sampling days.

Trajectories are occasionally ambiguous, for example, on July 5, 1995, when the average NSS concentration was 9.0 μg/m³ (the highest of the study). The sixth-day endpoint of the 0000 UT trajectory on July 6, 1995 lies to the northwest, in the middle of the North Atlantic. Prior to this, on days 7, 8 and 9, the trajectory came from the northwest in the North Atlantic. The sixth-day endpoint for the trajectory begun 12 hours later (1200 UT July 6, 1995) is at the same location as that of the 0000 UT trajectory. Previous to this point, the 1200 UT trajectory came from the northeast in central Europe. This trajectory, rather than the one begun 12 hours earlier, is more consistent with the high NSS concentration measured on July 5, 1995. The difference between the two trajectories is due to a frontal passage. The geographical uncertainty corresponds in time

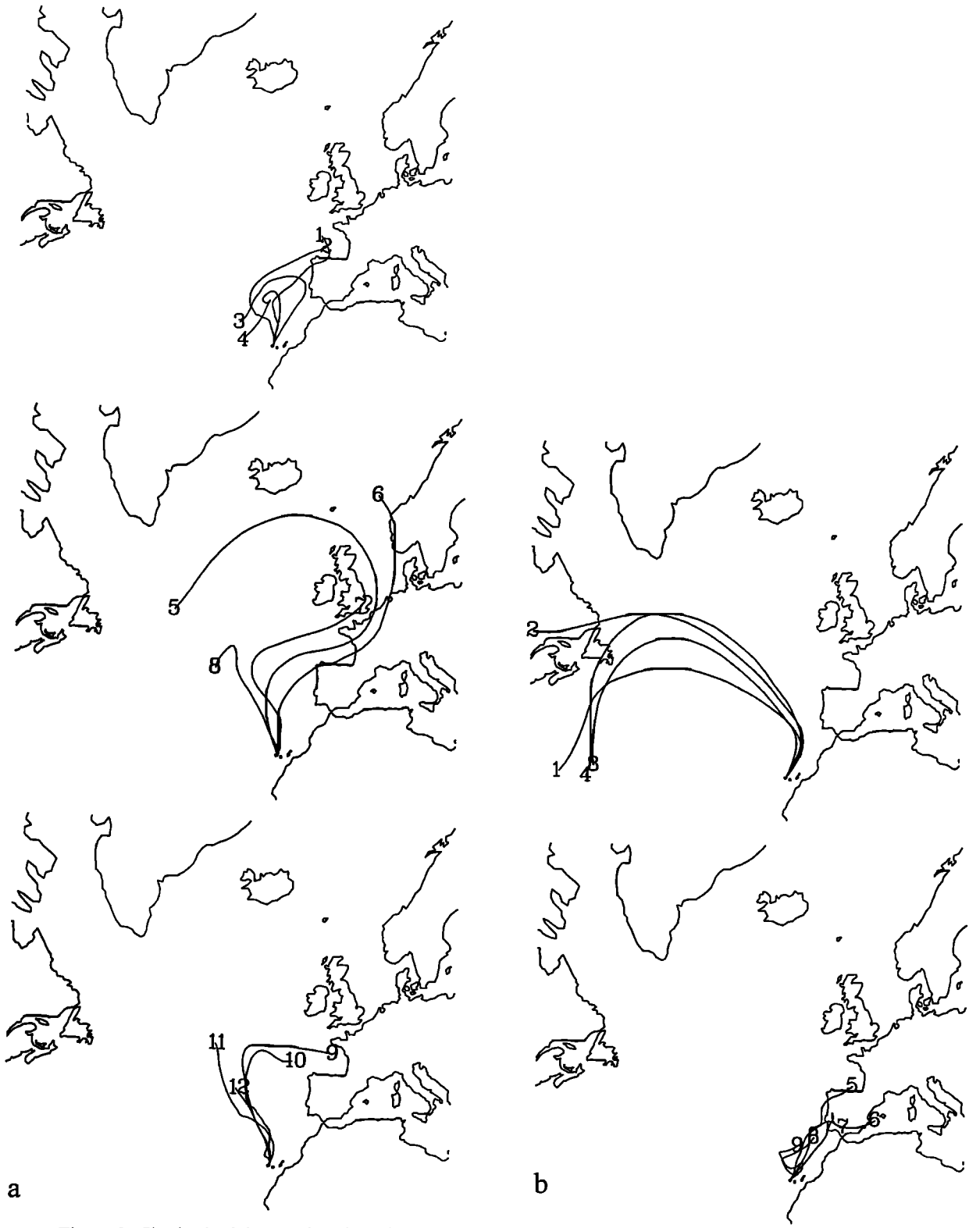

Figure 2. Six-day back isentropic trajectories from Pico del Ingles (992 m AMSL) for sampling days in 1995 and 1996, with average non-sea-salt sulfate ($\mu g/m^3$) given in parentheses. (a) 1995: (trajectory 1) June 10 (7.7); (trajectory 2) June 11 (3.3); (trajectory 3) June 22 (2.8); (trajectory 4) June 23 (1.67); (trajectory 5) June 25 (5.1); (trajectory 6) June 27 (7.5); (trajectory 7) June 29 (2.7); (trajectory 8) June 30 (2.2); (trajectory 9) July 1 (4.3); (trajectory 10) July 2 (4.8); (trajectory 11) July 5 (9.0); (trajectory 12) July 7 (5.0); (b) 1996: (trajectory 1) July 4 (0.69); (trajectory 2) July 6 (0.84); (trajectory 3) July 7 (1.29); (trajectory 4) July 8 (0.40); (trajectory 5) July 17 (2.7); (trajectory 6) July 18 (6.8); (trajectory 7) July 19 (6.9); (trajectory 8) July 24 (6.1); (trajectory 9) July 25 (1.75).

to 72±12 hours and gives rise to diametrically opposed source areas. The 0000 UT trajectory points to a clearly inappropriate source area. However, with knowledge of the pollution chemistry and further meteorological analysis, it becomes clear that the source of air impacting this sample was Europe, not the open ocean.

3.3. In Situ Cloud Microphysics

The relationship between droplet concentration and number-weighted mean diameter (MD) is shown in Figure 3. Cloud liquid water content (LWC) may vary in part due to variations in the height of the sampling site above cloud base for a given cloud temperature. The data in Figure 3 are stratified according to LWC into three classes based on the mean LWC (MLWC) and its standard deviation (s): (1) LWC < MLWC - 1 standard deviation; (2) MLWC - 1 standard deviation ≤ LWC ≤ MLWC + 1 standard deviation; and (3) LWC > MLWC + 1 standard deviation. Droplet concentrations ranged from about 100 to over 1000 cm^{-3}. The higher concentrations are typical of continental (polluted), not remote marine conditions (<100 cm^{-3}). The variation in droplet size for a given droplet number concentration may reflect variations in the height of cloud base with respect to the sampling site. These variations are small compared with the overall variation in the plot, and droplet size distribution variations during a given sampling period were slight. Observations made driving up and down the mountain before and after sampling indicated the cloud base was typically 100 to 200 m below the site. Note that while variations in LWC due to changes in height above cloud base should be random with respect to the initial droplet size distribution, most of the high-LWC cases are associated with larger droplet numbers and smaller droplet sizes.

Figure 4a demonstrates a weak (r = 0.37) but significant relationship between LWC and droplet number concentration. Although the precipitation mode droplet size distribution was not measured, this relationship is consistent with inhibition of droplet coalescence and precipitation in clouds with small, narrow droplet size distributions [*Albrecht*, 1989]. Further evidence for this effect is given in Figure 4b, which again demonstrates a significant correlation (r = 0.60) between mean droplet size and the relative width of the size distribution (coefficient of variation).

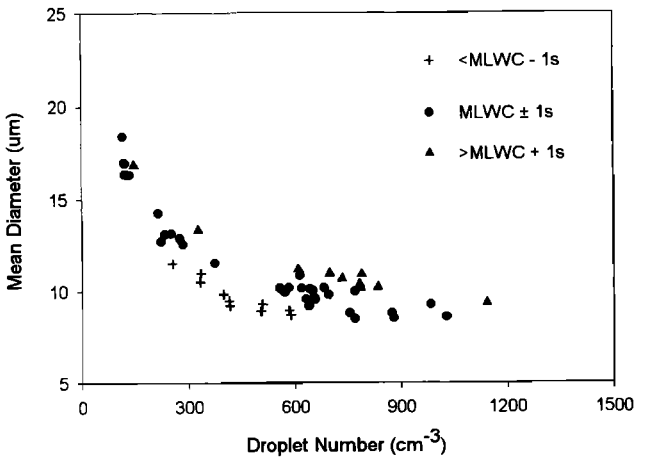

Figure 3. Cloud droplet mean diameter (MD) versus cloud droplet number concentration in three ranges of liquid water content.

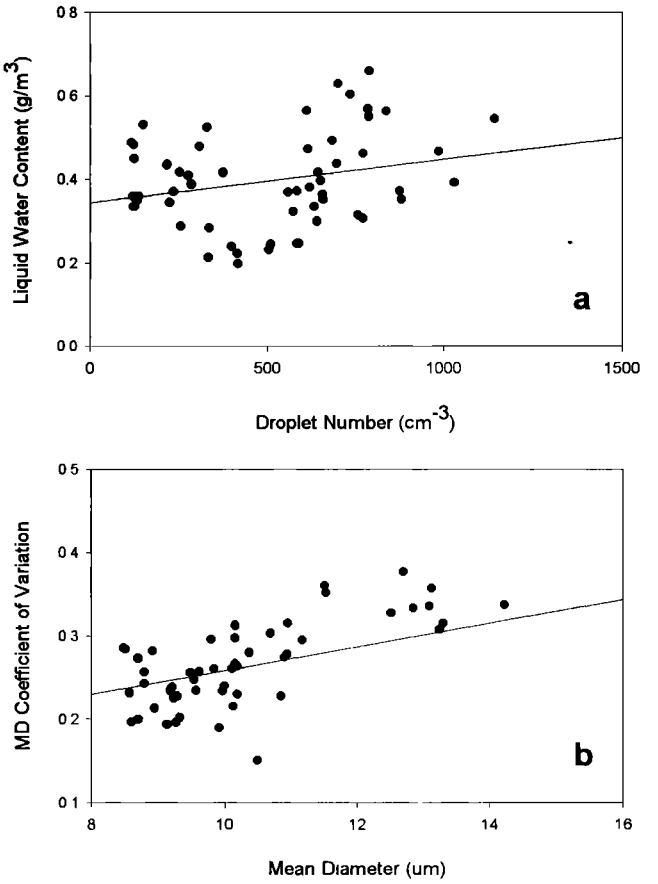

Figure 4. (a) Cloud droplet number concentration versus cloud liquid water content. (b) Cloud droplet mean diameter (MD) versus the relative width of the cloud droplet size distribution (coefficient of variation).

3.4. Microphysical-Chemical Relationships

The relationships between droplet number concentration and clear air concentrations of NSS, nitrate, Na^+, and EC are shown in Figures 5a-5d. Sodium is assumed to be a surrogate for the precloud sea-salt aerosol. Direct relationships are evident between droplet number and NSS and nitrate. Four samples collected on June 25, 1995 (indicated in the plots by pluses) exhibited moderate NSS and nitrate concentrations but also the highest droplet number and sea-salt concentrations of the study. Excluding these four samples, the correlations between droplet number and NSS and nitrate were 0.92 and 0.83, respectively. Including the high-Na samples, the droplet number-Na correlation was 0.54; without these samples, the correlation decreased to 0.10.

Figure 5d shows the relationship between droplet number and elemental carbon concentration. Excluding two outliers (shown in Figure 5d and Figure 1) but including the high Na (sea-salt) samples, the correlation between droplet number and EC concentration was 0.74. If it is assumed that EC is insoluble, its presence in the droplets and correlation with droplet number suggests that

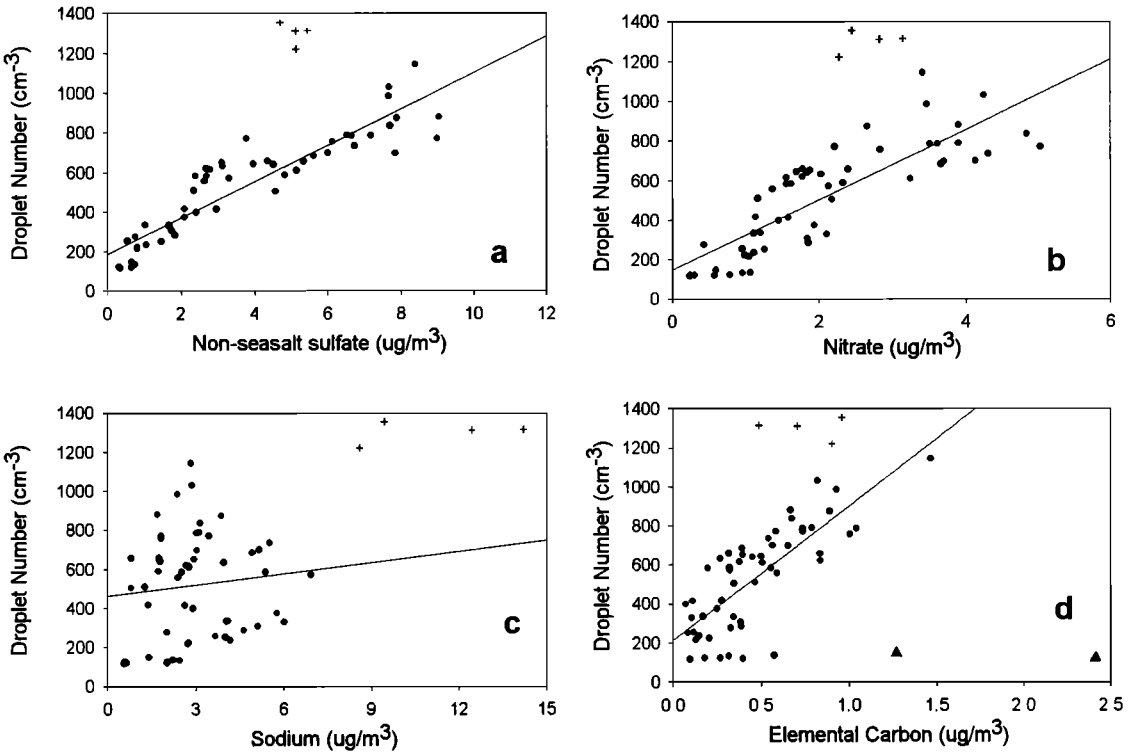

Figure 5. Cloud droplet number versus concentrations of (a) non-sea-salt sulfate, (b) nitrate, (c) sodium, and (d) elemental carbon (sea-salt episode of July 25, 1995 represented by pluses).

EC was internally mixed with at least one other soluble aerosol component. Although EC and NSS sulfate appeared moderately correlated, the soluble species with which EC was internally mixed could also have been nitrate or organic carbon, for example.

Raes [1996, p. 750] noted, "It is not yet possible to treat (multidimensional) aerosol distributions as prognostic variables in global climate models (GCMs) and do an 'ab-initio' calculation of the effects of aerosols" and asked, "Are there useful empirical correlations between the mass concentration of individual aerosol components and the radiative and cloud nucleating properties of that same aerosol?". Current estimates of both direct and secondary ("Twomey effect") aerosol radiative forcing, by, for example, *Kiehl and Briegleb* [1993] and *Boucher and Lohman* [1995], respectively, have been based on empirically derived "mass effect" relationships and/or "assumptions regarding the aerosol size distribution" [*Raes*, 1996].

Table 2. Average Microphysical and Chemical Properties for 1995 and 1996

Property	1995	1996
MD[a]	9.4±0.6	12.9±2.7
Number[b]	764±275	384±246
NSS[c]	4.7±2.2	2.8±2.6
Na^{+}[c]	3.8±3.3	3.2±1.5

Values represent the average and standard deviation.

[a] Number-weighted mean droplet diameter (μm).

[b] Droplet number concentration (cm^{-3}).

[c] Clear air equivalent concentration ($\mu g/m^3$).

Van Dingenen et al. [1995] compiled data from studies in Tasmania, Puerto Rico, Washington State, the Azores, Whiteface Mountain, New York, and Ontario, Canada, relating NSS concentrations in aerosol particles and cloud droplets to CCN and cloud droplet numbers. Combining all of these data, the relationship between NSS and number concentration (N) was

$$\log(N) = 2.33 + 0.40 \log(NSS). \quad (r^2 = 0.42) \qquad (1)$$

Excluding the high-sea-salt episode, the corresponding relationship exhibited by the Tenerife data is

$$\log(N) = 2.38 + 0.64 \log(NSS). \quad (r^2 = 0.90) \qquad (2)$$

Although the Tenerife droplet number and NSS concentrations span the ranges found in the previous studies, the slope is higher for the Tenerife data and the relationship is much less variable. The higher slope for the Tenerife data could be due to significant amounts of other soluble species such as nitrate, whose concentrations correlate with that of NSS (Figure 1), or unaccounted-for soluble material such as organic carbon.

The chemical and microphysical data also indicate clear differences between years. Average mean diameter, droplet number concentration, and NSS and Na^{+}concentrations are presented along with their standard deviations for 1995 and 1996 in Table 2. The droplets were smaller and more numerous, with higher NSS concentrations, in 1995. These differences are statistically significant (α=0.05, two-tailed t test). The year-to-year differences in average sodium concentrations are not significant. Thus, if our samples were representative, the MBL near Tenerife was more polluted in 1995 than in 1996.

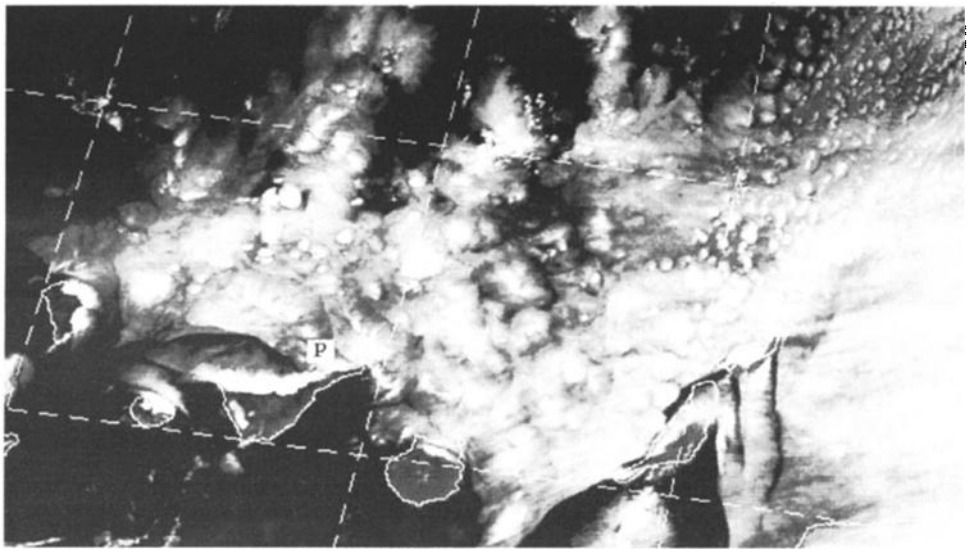

Figure 6. AVHRR 14 visible satellite image for 1500 UMT on July 18, 1996. The coast of northeastern Africa is shown with coastal outline on the extreme right. The location of the Pico del Ingles sampling site on the northern tip of the island of Tenerife is indicated by P. Dashed lines correspond to a latitude/longitude grid at 2 degree intervals.

3.5. Satellite Observations and Droplet Size Estimates

Satellite multispectral image data obtained on the afternoons and evenings of two sampling dates, July 8, 1996 and July 18, 1996, were used to examine the spatial variability of cloud physical characteristics offshore and at the sampling site, and these analyses were also applied to radiative transfer model calculations of the shortwave forcing associated with observed changes in droplet size. The first case represents a day with airflow from the west (trajectory 4 in Figure 2b), low aerosol NSS concentrations, low droplet number concentrations, and large droplet size, while the second day was a characteristic example of an air mass with flow from Europe (trajectory 6 in Figure 2b), very high values of NSS and droplet number concentrations, and a small droplet size. An example of the regional cloud distribution observed during these case studies is shown by Figure 6, an AVHRR 14 visible image for the afternoon (1500 UT and 1600 local time) of July 18. The upwind stratus and stratocumulus fields indicate a typical northeasterly airflow. Cloud similar to that offshore is observed above the sampling location at Pico del Ingles (northern tip of Tenerife), while downwind of this area the island causes significant modification in the cloud field. The afternoon satellite image data provided shortwave reflectance characteristics from which cloud droplet sizes were obtained. Evening overpass image data from the AVHRR satellite (available at 2000 local time) do not provide usable shortwave reflectance information, but the enhanced thermal and low-light visible images on these evenings did indicate the cloud field to be relatively constant over the afternoon-to-evening time period, with some increase in cloud layer uniformity.

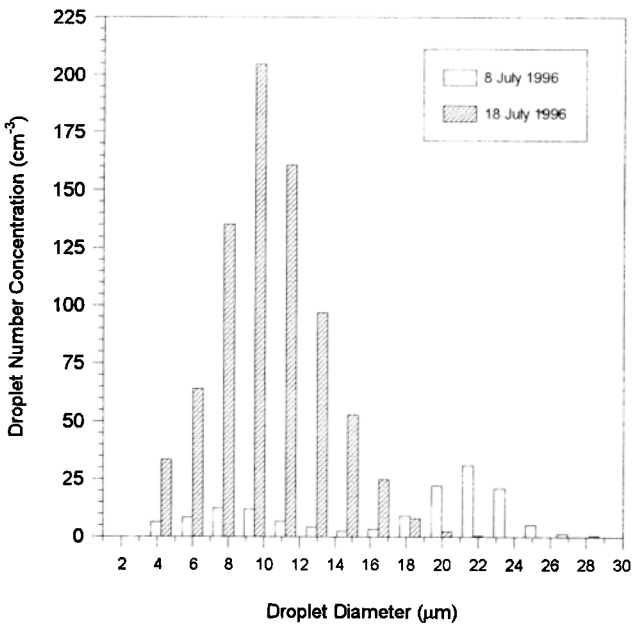

Figure 7. Cloud droplet size distributions for a clean (July 8, 1996) and a polluted (July 18, 1996) day.

We make the assumption that daytime cloud satellite measurements can be directly compared with nighttime in situ microphysical measurements because of the relative constancy of the cloud field between late afternoon and evening as observed in the satellite imagery, the small variation in measured cloud microphysical and chemical properties observed during the 3-hour sampling periods, and the spatial uniformity in droplet sizes retrieved from the afternoon satellite multispectral data for clouds offshore, upwind, and over the sampling site. For the July 8 case, in situ measurements indicated low droplet number and NSS concentrations (127 cm^{-3} and 0.40 $\mu g/m^3$, respectively) and large droplet size (effective radius 10.5 μm). This was contrasted with the July 18 sampling period during which the average in situ droplet number and NSS concentrations were 786 cm^{-3} and 6.8 $\mu g/m^3$, respectively, and the average droplet effective radius was 6.0 μm. Time-integrated droplet size distributions for the evening

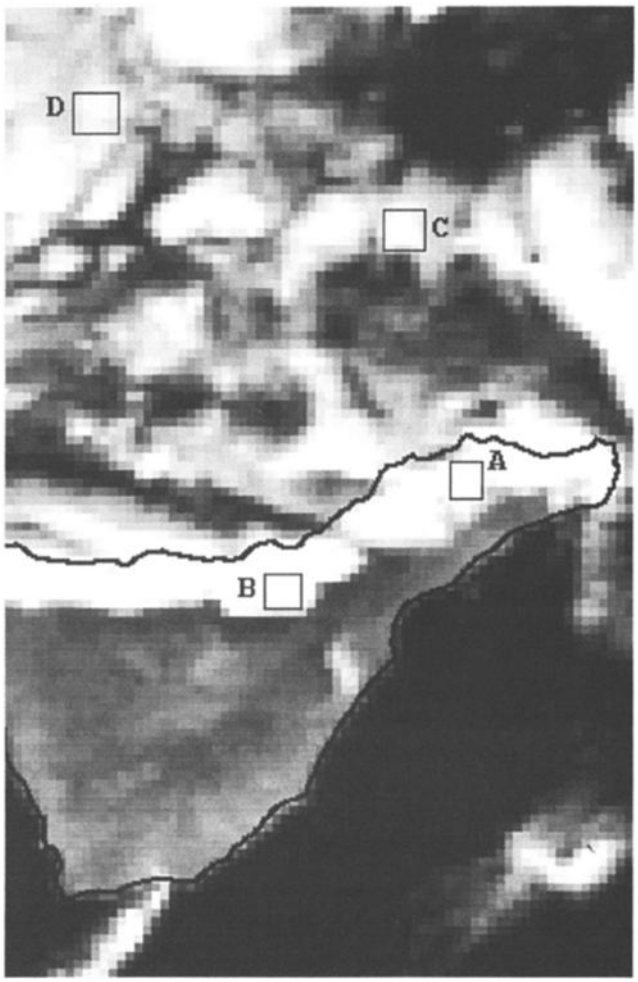

Figure 8. AVHRR 14 visible image for July 8, 1996. Outlined box areas are Pico del Ingles (box A), upslope cloud blocked by the El Teide orography (box B), offshore marine stratocumulus (box C), and offshore marine stratus (box D).

sampling periods on each of these days are presented in Figure 7. The size distribution for July 8 has concentration modes at diameter values of both 7-8 μm and 21-22 μm, while the July 18 population has a single concentration mode at 9-10 μm with very few droplets larger than 20 μm. Drizzle was visually observed during the in situ sampling period at Pico del Ingles on July 8 but not on July 18. Within-day values of the coefficient of variation of cloud droplet number and NSS concentrations obtained from the in situ measurements were 11% and 4% respectively for July 8 (during sampling period 1900-2100 UT) and were 0.3% and 4% respectively, for July 18 (sampling period 1815-2015 UT). These observations suggest that the aerosol affecting the clouds within the air mass was quite different between the two case studies, but was relatively uniform during each individual day, over timescales of hours and distances of hundreds of kilometers.

Satellite multispectral image data can be used to evaluate the similarity in cloud sampled at Pico del Ingles with other clouds in the vicinity, including those over the open ocean. Figure 8 is a visible image sector for 1500 UT on July 8 for the immediate area of Tenerife. Boxes identify sampling areas of 30-36 km^2, from which 25-30 pixels were extracted in each of the AVHRR 14 image channels. The horizontal dimension of the sampling boxes in the figure is approximately 6 km. Box A covers the sampling site at Pico del Ingles, which shows cloud formed by marine airflow and cloud formation over the ridge but within the MBL. A contrasting cloud area of optically thicker cloud (box B) is formed by orographically restricted flow. In this area, the high volcanic ridge which is the northern flank of the El Teide volcano (elevation 3715 m AMSL) extends through the marine inversion and blocks the northeastern flow within the MBL. This cloud has a more recurrent and persistent nature and is possibly influenced by afternoon heating of the west facing slopes. The underlying coastal region is also heavily populated, such that the cloud may contain pollutant aerosol produced on the island.

Two offshore cloud areas (box C and box D) were selected to represent stratus and stratocumulus formed over the ocean in the same air mass reaching the sampling site, perpendicular to the northeast trade wind flow which passes over Pico del Ingles. Box C appears to be an area of marine stratocumulus, while box D represents an optically thinner stratus area. Figure 9 shows a scatterplot of the visible and near-infrared radiance data values of the four cloud areas (A-D), as well as radiative transfer model results (curves) for specified cloud microphysical conditions. The curves in Figure 9 are radiative model results for the AVHRR 14 channel 1 visible reflectance and channel 3 equivalent blackbody temperature of a simulated cloud layer with a range of values for droplet effective radius, and the position of the image pixel data points can be used to estimate which cloud droplet size matches the image area bispectral characteristics. The model curves also demonstrate the effects of the underlying ocean versus land surface reflectance and near-infrared emission, for cloud with a droplet effective radius of 10 μm. As cloud optical thickness (and visible reflectance) increases, the surface characteristics have a reduced influence on the near-infrared brightness temperature. Thus, for pixels which have a channel 1 reflectance above approximately 40%, the channel 3 brightness temperature approaches an asymptotic value which is indicative of the cloud scattering signature due to droplet size variations.

The locations of the scatterplot points in Figure 9 indicate that the cloud observed during the late afternoon of July 8 over Pico del Ingles (box A) has an effective radius of 9.5 μm, while the oceanic cloud areas (box C and box D) have values of 10-11 μm. The in situ measurements at Pico del Ingles provided a cloud droplet size of 10.5 μm during the sampling period (2000-2130 UT), within ~1 μm of the value retrieved from the afternoon satellite data. Identical results (effective radius of 9.5-10.5 μm) were also obtained by estimating cloud droplet size for the area in the satellite image data which was directly upwind (NE) of the Pico del Ingles site, at the distance which would have been traveled by the air mass within the time period between the satellite overpass time and the in situ sampling time at Pico del Ingles. Finally, note that pixel samples shown in Figure 9 for box B suggest a significantly smaller droplet size (5-7 μm) for the cloud formed below the El Teide ridge, which may be related to local aerosol sources.

Table 3 summarizes the comparison of effective radius of cloud droplet size distributions and other physical parameters obtained during the in situ microphysical measurements with satellite-estimated values for July 8 and for the second case (July 18). The

Table 3. Summary of measured concentration of non-sea-salt sulfate (NSS), droplet number concentration (N), liquid water content (LWC), and droplet effective radius (R_e) for Pico del Ingles, with satellite-derived droplet effective radius for Pico del Ingles (Box A) and other image areas, for contrasting case studies selected from the field project periods.

Date	In situ Measurements				Satellite-derived R_e, μm			
	NSS, μg m^{-3}	N, cm^{-3}	LWC, g m^{-3}	R_e, μm	Box A	Box B	Box C	Box D
July 8, 1996	0.4	127	0.48	10.5	9.5	6.0	10.0	10.5
July 18, 1996	6.8	786	0.59	6.0	5.0	6.0	5.0	5.0

data in this table represent evidence that the lower aerosol concentration on July 8 is associated with smaller droplet concentration, lower liquid water content, and larger droplet size, which was observed by both in situ sampling and by satellite analysis of clouds over the adjoining ocean and over the sampling site.

Figure 10 is a visible image sector for 1500 UT on July 18, 1996, extracted from the larger area shown in Figure 6, with sample box areas analogous to those depicted in Figure 8. Figure 11 presents the satellite image reflectance and brightness temperature values for pixels withing these sampling boxes, as well as model-calculated curves for these satellite channel characteristics at this image time. The scatterplot points in Figure 11 clearly show the that cloud over Pico del Ingles (box A) has the same bispectral signature and estimated droplet size as cloud in box C. The stratus area represented by box D suggests a slightly smaller droplet size, but all three areas indicate uniform cloud with effective radius of 5 μm (±0.5 μm). As with the previous case, we also examined the pixel characteristics of the cloud layer directly upwind of Pico del Ingles at a distance that corresponds to the wind direction (NE) and wind speed (7 m s^{-1}) observed on this day. The marine stratocumulus in that area yielded the same value (5 μm) as estimated at Pico del Ingles, and within 1 μm of that obtained from the in situ microphysical data.

The points for box B have a distinctly different character than the other areas, and at the same time match the same box B pixel characteristics observed on July 8. This suggests that the conditions that form clouds in that area are not responding in the same manner to the aerosol concentration in the upwind marine air mass, which does change significantly between the two dates. The estimated droplet size in this area is relatively small for both days, indicating the aerosol effect on cloud may be strongly influenced by orographic blocking of airflow in the MBL and local pollution sources.

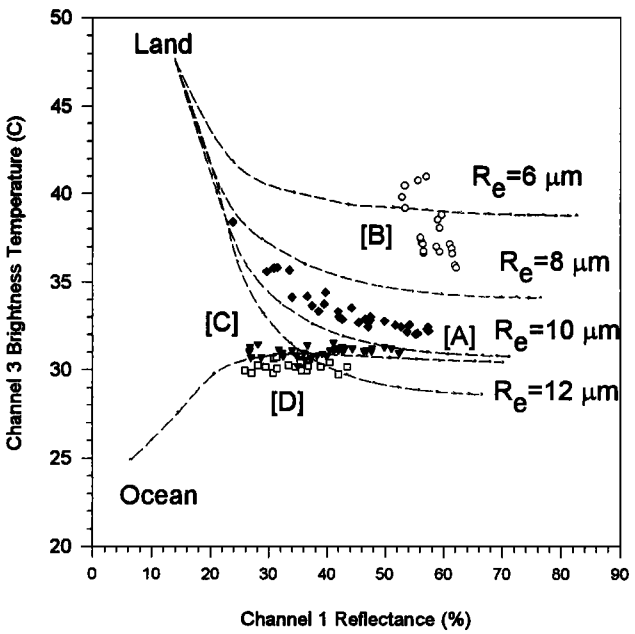

Figure 9. Case study results for July 8, 1996 of AVHRR 14 channel 1 reflectance and channel 3 brightness temperature for cloud areas represented by areas A - D in Figure 8, and for model curves with the indicated droplet effective radius (R_e).

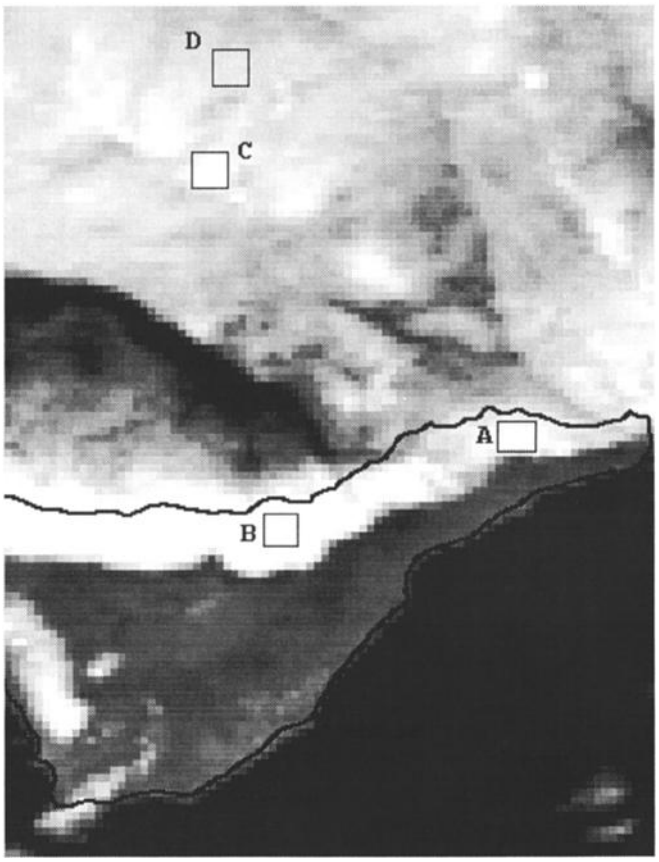

Figure 10. AVHRR 14 visible image for 1500 UT on July 18, 1996. Outlined boxes A-D correspond to cloud areas described in Figure 8.

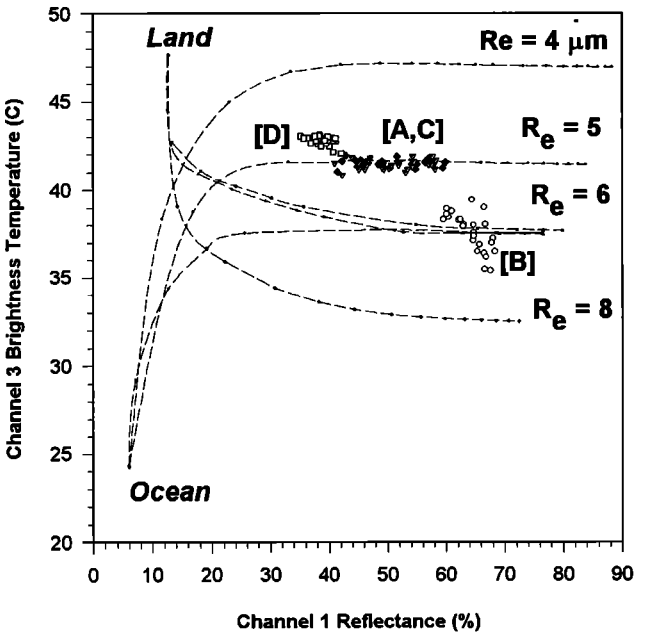

Figure 11. As in Figure 9, for July 18, 1996.

There are small uncertainties for the droplet size estimates in the use of the satellite data (due to the time difference of sampling, the assumption of a vertically homogenous cloud layer, and the satellite data calibration) and in the application of the radiative transfer model. Two model curves are also shown for effective radius values of 6 μm, to demonstrate one effect of model parameter uncertainty. The radiative transfer model calculates the channel 3 brightness temperature with input of a cloud top temperature derived from the AVHRR thermal channel data, and there is an uncertainty of approximately 1°C in this value due to variation in upwelling radiance (primarily due to water vapor) in the optical path between cloud top (above the inversion) and the satellite. The two model curves converging at an effective radius of 6 μm were calculated for two different values of cloud top temperature (and assuming identical land surface temperature). The lower and upper curves of this pair were calculated for cloud top temperatures of 14° and 15°C, respectively. This effect on derived droplet size is small but is one possible reason for differences between satellite-derived droplet size estimates and in situ measurements of droplet size.

The two cases (July 8 and July 18) presented here show a correspondence between the satellite-retrieved droplet sizes for cloud sampled over Pico del Ingles and stratiform cloud over the open ocean in the vicinity of and directly upwind of the island. There was also agreement between the satellite-derived droplet sizes and the in situ measurements taken 4-5 hours later. Comparisons between measured and estimated droplet effective radius indicate agreement within 1 μm over the Pico del Ingles sampling site, and between the open ocean and Pico del Ingles, for both case studies. At the same time, the difference in droplet effective radius on the two days is large, showing a decrease from 10 μm on July 8 to 6 μm on July 18, corresponding to an increase in NSS aerosol concentration by more than tenfold, and a threefold increase in satellite-derived aerosol optical thickness. Therefore, it is apparent that changes in cloud microphysical conditions due to aerosol concentration in the marine air mass are represented by in situ sampling at Pico del Ingles.

3.6. Model Calculations of Cloud Radiative Forcing

The influence of the satellite-derived droplet size changes on cloud radiative forcing was examined by radiative transfer modeling. For both cases described above, broadband radiative fluxes at the top of the atmosphere were calculated using the two-stream flux component of the streamer model [*Key*, 1996], in which cloud optical properties and atmospheric gas and aerosol extinction are parameterized over 24 shortwave and 105 longwave spectral bands. Satellite-derived values of aerosol optical depth were obtained from the AVHRR data [*Durkee et al.*, 1986]. Typical values of aerosol optical depth were 0.05 on July 8 and 0.14 on July 18, which is consistent with the elevated droplet number and NSS concentrations on July 18. Cloud top temperature was specified by a two-channel correction using the AVHRR thermal channels. In situ sampling provided the cloud droplet size and cloud liquid water content information. The resulting values of upward shortwave flux in cloudy versus clear model simulations were used to calculate shortwave cloud forcing (SWCF), defined as the difference between net fluxes (W m^{-2}) at the top of the atmosphere with and without the presence of the cloud layer.

Figure 12 shows results of SWCF calculations for the microphysical and aerosol optical depth conditions observed on July 18, 1996 (effective radius = 6 μm) and on July 8, 1996 (effective radius = 10 μm), and two types of aerosol vertical profiles (discussed later), calculated in mid-afternoon (solar zenith angle defined from satellite image time in Figure 6). The magnitudes of the values of SWCF demonstrate the significant effect of marine cloud in controlling the daytime radiative budget over the ocean. The difference between the results for the different droplet sizes is also quite large, showing an 8% increase in SWCF for cloud optical depth of 12 (typical of the sampled cloud) as droplet effective radius decreases from 10 to 6 μm. While the daily total

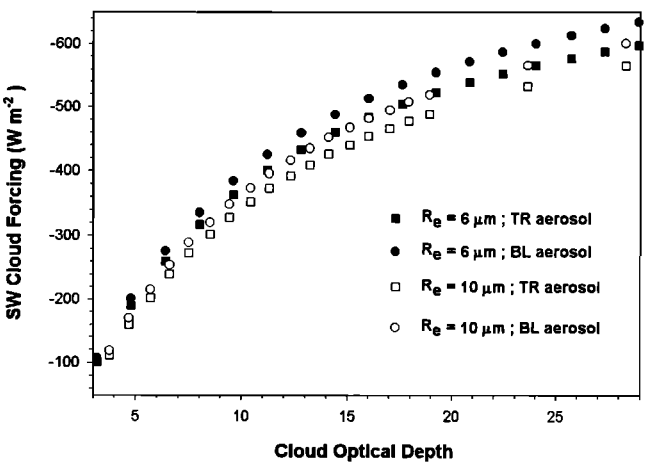

Figure 12. Shortwave cloud radiative forcing for July 8, 1996 (clean) and July 18, 1996 (polluted) model conditions with differing cloud droplet effective radius (R_e) and vertical distribution of the aerosol throughout the troposphere (TR) or primarily in the marine boundary layer (BL).

SWCF varies as a function of solar illumination, fractional cloud cover, and diurnal fluctuations in cloud microphysical conditions, these results demonstrate the large day-to-day shifts in radiative forcing which can be associated with pollution aerosol sources and their effect on clouds.

The vertical profile of aerosol also influences the magnitude of SWCF. Total aerosol optical thickness can be obtained from satellite data, but information on the vertical distribution of this aerosol is typically unknown. Aerosol layers can be transported above the boundary layer from source regions or become resident in the free troposphere by mixing at the boundary layer interface. Figure 12 shows curves for which the aerosol was concentrated in the boundary layer (BL), designated by the solid and open squares, while aerosol distributed more evenly throughout the troposphere (TR) is shown by circles. The total aerosol optical thickness in each case is 0.14, as derived from the AVHRR satellite data for the July 18, 1996, case, selected merely as an example date for which a polluted air mass was apparently transported from Europe. The aerosol optical extinction characteristics were assumed to be those of an anthropogenic (urban) aerosol type, although the chemical and size distribution characteristics of the aerosol population are certain to have undergone some modification during transport from Europe. The case in which the satellite-observed aerosol optical thickness is distributed throughout the troposphere allows the aerosol to intercept a greater portion of the upward and downward solar radiation above cloud top and diminishes the effect of the cloud layer on SWCF. The same effect can be caused by aerosol located within the stratosphere, but this condition is more readily accounted for by other satellite methods of mapping stratospheric aerosol. It is important to note from these results that the magnitude of this influence is comparable to that of a change in droplet size. Thus, information on the presence of aerosol above cloud top is necessary for adequate distinction of the cloud microphysical versus aerosol layer impacts on broadband net flux.

Putaud et al. [1996] presented results from pre-ACE-2 (Aerosol Characterization Experiment) measurements obtained on Tenerife during July 1995. Aerosol NSS concentrations were measured at Izana, a free tropospheric monitoring site at 2370 m AMSL, and at Punta del Hidalgo, located at sea level on the northern coast approximately 10 km from our sampling site. On July 5 and July 21, 1995, when NSS concentrations at Punta del Hidalgo were at monthly maxima of 6.7 and 5.8 $\mu g/m^3$, respectively, corresponding concentrations at Izana were significantly smaller (0.5 and 1.4 $\mu g/m^3$, respectively). Had the aerosol vertical distribution been similar for our polluted case (July 18, 1996), SWCF would not have been substantially diminished by aerosol above the boundary layer. Other cases may show more or less modification by upper-level aerosol of the effect of boundary layer aerosol on marine cloud radiative forcing.

4. Discussion

It is evident from the high concentrations of NSS and nitrate and the air mass back trajectories that the study area was highly polluted during the experiment and that Europe was the likely pollution source. If it is assumed that all of the nitrate was pollution-derived, then NSS sulfate can be apportioned to anthropogenic and natural biogenic sources by regressing its concentrations against those of nitrate and MSA, which is biogenic in origin. The regression was weighted by the "effective variances" [*Watson et al.*, 1984] to provide for unbiased estimates in the presence of independent variable measurement uncertainty. This resulted in the following relationship:

$$\text{NSS} = 1.69\ (\text{nitrate}) + 4.53\ (\text{MSA}) \quad (r^2=0.96) \qquad (3)$$

Applying (3) to the average nitrate and MSA concentrations (2.12 and 0.080 $\mu g/m^3$, respectively) results in an average estimated NSS concentration of 3.94 $\mu g/m^3$, compared with the measured average concentration of 3.72 $\mu g/m^3$. Ninety-one percent (3.58 $\mu g/m^3$) of the average estimated NSS was pollution-derived while 9% (0.36 $\mu g/m^3$) was biogenic. This is consistent with previous marine background measurements in the northern hemisphere [*Bates et al.*, 1992].

Hegg [1994] presented linear regressions of (non-log-transformed) CCN (measured at 1% supersaturation) on NSS (corresponding to (1) and (2) measured from aircraft at marine and coastal Atlantic and Pacific locations. The slopes varied widely, ranging from 0.13 off the Virginia coast to 117 in the northeast Pacific. The slope for the non-log-transformed Tenerife data corresponding to (2) is 91. For comparison, *Van Dingenen et al.* [1995] reported a (non-log-transformed) slope of 126, that is, larger than the Tenerife slope, for sulfate versus accumulation mode particle number on a North Atlantic transect between Halifax and the Canary Islands. While the corresponding log-log slope was 0.38, that is, smaller than the Tenerife log-log slope, the results of our Tenerife study are generally consistent with those of *Van Dingenen et al.* [1995].

Table 1 shows that the ratio of average nitrate to average NSS concentrations in cloud droplets was 0.57. *Huebert et al.* [1996] reported aerosol nitrate to NSS ratios of 0.66 at Santa Maria in the Azores. Gaseous nitric acid concentrations were 4% and 10% of particulate nitrate concentrations under clean marine and polluted conditions, respectively. It is therefore reasonable to conclude that most of the nitrate in Tenerife cloud water was associated with the precloud CCN (precloud aerosol particles) and not with absorption of gaseous nitrate into the cloud droplets. The close proximity of the sampling site to cloud base and the high nitrate-sulfate correlation (0.93) argues against significant postnucleation modification of the cloud droplet chemistry.

For nitrate to contribute significantly to CCN concentrations, it must be associated with the more-numerous fine, not large, particles. The high correlation of nitrate with NSS argues that nitrate is associated with the fine aerosol fraction. A nonsignificant correlation (0.12) of nitrate with sodium argues that nitrate was not associated with large sea-salt particles. The seawater Cl/Na mass ratio (1.8) in the cloud water also suggests nitrate did not replace chloride on sea-salt particles. It is possible, however, that nitrate was associated with larger geological dust particles, and that the correlation of nitrate with sulfate was due to a common continental source for both NSS and dust. It is therefore possible that pollution-derived nitrate contributed significantly to the nucleation properties of aerosols in this region. While soluble organics were not measured during this study, the results of *Novakov and Penner* [1993] and *Rivera-Carpio et al.* [1996] suggest that organic aerosols contribute significantly to CCN activity in the marine environment. Much of the variation previ-

ously observed in relationships between NSS and droplet, CCN, or aerosol number concentrations may be due to the presence or absence of significant amounts of soluble species other than NSS at different locations.

For empirical "mass effect" relationships, for example, NSS versus cloud droplet or CCN number concentration, to be useful as parameterizations in GCMs, explanations for their apparent variability are needed. One likely cause of the variability found in previous studies is the wide variation in the sources, transport distances, and processing of aerosols measured at different locations. The Tenerife measurements display much less variability for several reasons. The source region, Europe, is consistent and at a fixed average distance from Tenerife. Constant transport distance implies constant aging and processing of the aerosol (for example, addition of sulfate to particles through dry oxidation of SO_2, and particle growth due to in-cloud uptake and oxidation of SO_2 and agglomeration of droplets and/or further aerosol scavenging by droplets, followed by cloud evaporation), and variations over the long term can be viewed as random [*Lowenthal and Rahn*, 1989]. This leads to consistency in the shape of the CCN size distribution, with little variation in aerosol chemical composition; absolute concentrations are controlled by dispersion and removal during transport. Considering that for constant aerosol mass concentration, a 26% change in aerosol radius corresponds to a factor of 2 change in the aerosol number concentration, it is difficult to reconcile the lack of variation displayed in Figure 5a with significant variations of the aerosol size distribution or chemical composition.

Based on the back trajectory analysis, there was little or no influence of aerosol sources in North Africa on the cloud formed by marine airflow which was sampled on Tenerife. There were several periods of intense haze associated with flow from North Africa, but clouds were absent during these events because African air masses were extremely hot and dry. Significantly different circulation patterns in different years may nonetheless result in different relationships between precloud aerosol chemistry and cloud microphysical properties.

5. Conclusions

Two summer field campaigns conducted in 1995 and 1996 on the island of Tenerife in the Canary Islands have shown that pollutants transported from Europe have a strong influence on marine strati- form cloud chemistry and microphysics. Clear relationships between in situ cloud droplet size and number and pollutant concentrations provided evidence for the "Twomey effect". In two case studies representing polluted and clean conditions, satellite-derived cloud droplet sizes were similar for cloud offshore and upwind of the island, for cloud over an island sampling site, and for the in situ droplet size measurements at that site (taken 4-5 hours later). The effects of transported pollution aerosols on in situ cloud droplet number and size were consistent with a significant increase in shortwave radiative forcing inferred from satellite radiance measurements and radiative transfer model results. Clouds were conspicuously absent during periods of dust transport from North Africa. While African dust may play a significant role in direct aerosol shortwave radiative forcing, it apparently had little effect on cloud microphysical properties during our study. The observed annual variations in cloud microphysical and chemical properties illustrate the need for measurements in years with different atmospheric circulation patterns to elucidate the effects of anthropogenic and natural aerosols on marine cloud microphysics in this and other regions.

Acknowledgments. This work was supported by National Science Foundation grant ATM-9408660. Software for satellite image analysis was kindly provided by Peter Barber, Executive Director, Atmospheric Sciences Center at the Desert Research Institute. We wish to also acknowledge the assistance provided by Carmen Rus and her staff at the Spanish Weather Service in Santa Cruz de Tenerife. Special thanks also go to Ramon Juega of Meteography, Santa Cruz de Tenerife, for his assistance in logistical arrangements and governmental cooperation on Tenerife, without which this work could not have been conducted. We also recognize the special role of Olga Garro of the Desert Research Institute, who provided document and oral translation before and during the project to keep it running smoothly.

References

Albrecht, B., Aerosols, cloud microphysics, and fractional cloudiness, *Science*, 245, 1227-1230, 1989.

Baker, M.B., R.G. Corbin, and J. Latham, The influence of entrainment on the evolution of cloud droplet spectra, I, A model of inhomogeneous mixing, *Q. J. R. Meteorol. Soc.*, 106, 581-598, 1980.

Bates, T.S., J.A. Calhoun, and P.K. Quinn, Variations in the methanesulfonate to sulfate molar ratios in submicrometer marine aerosol particles over the South Pacific Ocean, *J. Geophys. Res.*, 97, 9859-9865, 1992.

Boucher, O. and U. Lohmann, The sulfate-CCN-cloud albedo effect: A sensitivity study with two general circulation models, *Tellus, Ser. B*, 47, 281-300, 1995.

Charlson, R.J., S.E. Schwartz, J.M. Hales, R.D. Cess, J.A. Coakley, Jr., J.E. Hansen, and D.J. Hofmann, Climate forcing by anthropogenic aerosols, *Science*, 255, 423-430, 1992.

Chow, J.C., J.G. Watson, L.C. Pritchett, W.R. Pierson, C.A. Frazier, and R.G. Purcell, The DRI thermal/optical reflectance carbon analysis system: description, evaluation and applications in U.S. air quality studies, *Atmos. Environ.*, 27A, 1185-1201, 1993.

Chow, J.C., J.G. Watson, E.M. Fujita, Z. Lu, D.R. Lawson, and L.L. Ashbaugh, Temporal and spatial variations of $PM_{2.5}$ and PM_{10} aerosol in the Southern California Air Quality Study, *Atmos. Environ.*, 28, 2061-2080, 1994.

Chuang, C.C., J.E. Penner, K.E. Taylor, A.S. Grossman, and J.J. Walton, An assessment of the radiative effects of anthropogenic sulfate, *J. Geophys Res.*, 102, 3761-3778, 1997.

Collett, J.L., B.C. Daube, and M.R. Hoffman, The chemical composition of intercepted cloud water in the Sierra Nevada, *Atmos. Environ.*, 24A, 959-972, 1990.

Durkee, P.A., D.R. Jensen, E.E. Hindman, and T.H. Vonder Haar, The relationship between marine aerosol particles and satellite-detected radiance, *J. Geophys. Res.*, 91, 4063-4072, 1986.

Harris, J.M. and J.D.W. Kahl, An analysis of 10-day isentropic flow patterns for Barrow, Alaska: 1985-1992, *J. Geophys. Res.*, 99, 25,845-25,855, 1994.

Hegg, D.A., Cloud condensation nucleus-sulfate mass relationship and cloud albedo, *J. Geophys. Res.*, 99, 25,903-25,907, 1994.

Hindman, E.E., E.J. Carter, R.D. Borys and D.L. Mitchell, Collecting supercooled droplets as a function of droplet size, *J. Atmos. Ocean. Technol.*, 9, 337-353, 1992.

Huebert, B.J., L. Zhuang, S. Howell, K. Noone, and B. Noone, Sulfate, nitrate, methanesulfonate, chloride, ammonium, and sodium measurements from ship, island, and aircraft during the Atlantic Stratocumulus Transition

Experiment/marine aerosol gas exchange, *J. Geophys. Res.*, 101, 4413-4423, 1996.

Jones, A., D.L. Roberts, and A. Slingo, A climate model study of indirect radiative forcing by anthropogenic sulfate aerosols. *Nature*, 370, 450-453, 1994.

Key, J., Streamer User's Guide, *Tech. Rep. 96-01*, 85 pp., Dep. of Geogr., Boston Univ., Boston, Mass.

Kiehl, J.Y., and B.P. Briegleb, The relative roles of sulfate aerosols and greenhouse gases in climate forcing, *Science*, 260, 311-314, 1993.

Lowenthal, D.H., and K.A. Rahn, The relationship between secondary sulfate and primary regional signatures in northeastern aerosol and precipitation, *Atmos. Environ.*, 23, 1511-1515, 1989.

Meier, W.N., J.A. Maslanik, J.R. Key, and C.W. Fowler, Multiparameter AVHRR-derived products for Arctic climate studies, *Earth Interactions*, EI009, 43 pp., 1997.

Munger, J.W., J. Collett, Jr., B. Daube, Jr., and M.R. Hoffman, Chemical composition of coastal stratus clouds: Dependence on droplet size and distance from the coast, *Atmos. Environ.*, 23, 2305-2320, 1989.

Novakov, T., and J.E. Penner, Large contribution of organic aerosols to cloud-condensation nucleus concentrations, *Nature*, 365, 823-826, 1993.

Putaud, J.-P., R. Van Dingenen, F. Raes, F. McGovern, M. Mangoni, J. Prospero, and H. Maring, Results of the pre-ACE-2 campaigns in the subtropical North Atlantic, in *Nucleation and Atmospheric Aerosols*, edited by M. Kulmala and P.E. Wagner, pp. 948-951, Elsevier Sci., New York, 1996.

Raes, F., Aspects of tropospheric aerosols: Questions and ACE-2, in *Nucleation and Atmospheric Aerosols*, edited by M. Kulmala and P.E Wagner, pp. 749-758, Elsevier Sci., New York, 1996.

Rivera-Carpio, C.A., C.E. Corrigan, T. Novakov, J.E. Penner, C.F. Rogers, and J.C. Chow, Derivation of contributions of sulfate and carbonaceous aerosols to cloud condensation nuclei from mass size distributions, *J. Geophys. Res*, 101, 19,483-19,493, 1996

Rogers, R.R., and M.K. Yau, *A Short Course in Cloud Physics*, third ed., 293 pp., Pergamon, Tarrytown, N.Y., 1989.

Savoie, D.L., J.M. Prospero, and E.S. Saltzman, Non-sea-salt sulfate and nitrate in trade wind aerosols at Barbados: evidence for long-range transport, *J. Geophys. Res*, 94, 5069-5080, 1989.

Schwartz, S.E., and M.O. Andreae, Uncertainty in climate change caused by aerosols, *Science*, 272, 1121-1122, 1996.

Stamnes, K., S.C. Tsay, W. Wiscombe and K. Jayaweera, Numerically stable algorithm for discrete-ordinate-method radiative transfer in scattering and emitting layered media, *Appl. Opt.*, 27, 2502-2509, 1988.

Twomey, S., The influence of pollution on the short-wave albedo of clouds, *J. Atmos. Sci.*, 34, 1149-1152, 1977.

Twomey, S., and J. Warner, Comparison of measurements of cloud droplets and cloud nuclei, *J. Atmos. Sci.*, 24, 702-703, 1967.

Twomey, S., M. Piepgrass, and T.L. Wolfe, An assessment of the impact of pollution on global cloud albedo, *Tellus*, 36B, 356-366. 1984.

Van Dingenen, R., F. Raes, and N.R. Jensen, Evidence for anthropogenic impact on number concentration and sulfate content of cloud-processed aerosol particles over the North Atlantic, *J. Geophys. Res.*, 100, 21,057-21,067, 1995.

Warner, J., The microstructure of cumulus cloud. Part II. The effect on droplet size distribution of the cloud nucleus spectrum and updraft velocity, *J. Atmos. Sci*, 26, 1272-1282, 1969.

Watson, J.G., J.A. Cooper, and J.J. Huntzicker, The effective variance weighting for least squares calculations applied to the mass balance receptor model, *Atmos. Environ.*, 18, 1347-1355, 1984.

Wetzel, M.A., R.D. Borys, and L. Xu, Analysis methods for land-based fog droplet size and optical depth using satellite data, *J. Appl. Meteorol.*, 35, 810-829, 1996.

R. D. Borys, D.H. Lowenthal, and M. A. Wetzel, Atmospheric Sciences Center, Desert Research Institute, P. O. Box 60220, Reno, NV 89506-0220. (e-mail. borys@dri.edu; dougl@dri.edu; wetzel@dri.edu.)

F. Herrera, A. Gonzalez, Department of Fundamental and Experimental Physics, University of La Laguna, La Laguna, Canary Islands, Spain. (e-mail: fherrera@ull.es; aglezf@ull.es.)

J. Harris, NOAA Climate Monitoring and Diagnostics Laboratory, 325 Broadway, Boulder, CO 80303-3328. (e-mail: jharris@cmdl.noaa.gov)

(Received December 3, 1997; revised June 11, 1998;
accepted June 16, 1998.)